General rational approximation of Gaussian wavelet series and continuous-time g_m-C filter implementation

Mu Li[1, 2] | **Yichuang Sun**[2]

[1]School of Information and Electrical Engineering, Hunan University of Science and Technology, Xiangtan, China
[2]School of Engineering and Technology, University of Hertfordshire, Hatfield, UK

Correspondence
Mu Li, School of Information and Electrical Engineering, Hunan University of Science and Technology, Xiangtan, China
Email: mli@hnust.edu.cn

Summary

A general method of rational approximation for Gaussian wavelet series and Gaussian wavelet filter circuit design with simple g_m-C integrators is presented in this work. Firstly, the multi-order derivatives of Gaussian function are analysed and proved as wavelet base functions. Then a high accuracy general approximation model of Gaussian wavelet series is constructed and the transfer function of first order derivative of Gaussian wavelet filter is obtained using quantum differential evolution (QDE) algorithm. Thirdly, as an example, a 5th order continuous-time analogue first order derivative of Gaussian wavelet filter circuit is designed based on multiple loop feedback structure with simple g_m-C integrator as the basic blocks. Finally, simulation results demonstrate the proposed method is an excellent way for the wavelet transform implementation. The designed first order derivative of Gaussian wavelet filter circuit operates from a 0.53V supply voltage and a bias current 2.5nA. The power dissipation of the wavelet filter circuit at the basic scale is 41.1nW. Moreover, the high accuracy QRS detection based on the designed wavelet filter has been validated in application analysis.

KEYWORDS

gaussian function, wavelet series, rational approximation, wavelet filters, g_m-C circuits

1 | INTRODUCTION

Over the last few years, the wavelet transform (WT) has played a significant role in mathematic analysis tools for non-stationary and transient signals, which is widely used in various application fields such as image processing, speech processing and signal processing, especially medical signal processing. The main advantage of the WT over the other classical transform is that it provides combined time and frequency localization[1, 2]. In some wearable and implantable medical devices, such as pacemakers[3-5], electroencephalograph[6-8] and cochlear implants[9, 10], the wavelet transform potentially has a large number of useful application. The common requirement for these devices is that they impose strict constraints on the power consumption, especially for the sensing circuit of implantable device, which is always active and for which the battery is hard to be replaced. Therefore, the power consumption of these medical devices is an important factor in design and manufacture. For a low power consumption perspective, many scholars and engineers used analog

circuit to implement the WT, and the better effect is obtained in practical applications.

The implementation of analog WT is divided into two stages: wavelet base approximation and wavelet filter circuit design. Wavelet basis functions are usually not directly implemented because they are non-causal. Hence, the rational approximation of wavelet function is the first problem to be solved. Some approximation methods have been proposed in the literatures, including time domain and frequency domain approximation. Among them, the time domain approximation method mainly includes L_2 approximation[11] and optimal algorithm approximation[12-14]. The frequency domain approximation is Padé[5], Maclaurin [6, 15, 16] and improved Maclaurin method[17]. In general, the time domain approximation method is more accurate than the frequency domain method because the fundamental expression of the wavelet is a time domain function. However, a common problem is that these studies are mostly focused on one type of wavelet base, while few studies are involved in a certain wavelet series. In fact, the general approximation method of wavelet function series is very significant and important to select the optimal wavelet base and implement analog WT. In addition, for the wavelet filter circuit design, some circuit design methods based on different structures such as cascade and multiple loop feedback prototype, and the basic building blocks such as log-domain[5, 12], switched current (SI) [13, 14], switched capacitor (SC)[18], current mirror[19] and operational transconductance amplifier (OTA, i.e. g_m)[4, 15-17]are proposed. Furthermore, for analog filter design, besides the basic blocks mentioned above, there are many other basic building blocks that can be selected such as current conveyor[20], source-follower[21, 22] and CMOS mixed-integrator[23, 24], etc. For log-domain circuit, the signal is nonlinearly compressed and expanded at the input and output terminal, respectively. In order to make the log-domain circuit characteristics linear, the dynamic range of the circuit is very limited. The drawback of SI and SC circuit is that working frequency is limited by Nyquist's theorem and sampling frequency. Moreover, there are aliasing effect and clock feedback problems in the SI and SC circuit. The main disadvantage of current mirror block is that it is difficult to match MOSFETS for use as mirrors. Compared with other candidate basic building blocks for high-order wavelet filter design, the g_m-C has advantages in operating frequency, circuit structure and parameter adjustment. Therefore, the g_m-C circuit design approach of wavelet filter is attracting attention. However, the structures and basic block of the wavelet filter based on g_m-C circuit usually are relatively complex so that the wavelet filter circuit design is more difficult.

In this work, a general relational approximation of Gaussian wavelet series and the inverse-fellow-the-leader-feedback (IFLF) structure wavelet filter with simple g_m-C integrator as the basic building block is presented. Firstly, Gaussian function and its multi-order derivative series are mathematical analyzed and the Gaussian series functions are proved to be wavelet bases. Then, a general time domain approximation model of the Gaussian wavelet base is structured according to the linear system theory. Subsequently, the optimal solution of the model is achieved by using QDE algorithm in order to obtain rational approximated transfer function of first order derivative of Gaussian wavelet filter. Thirdly, the 5th order Gaussian wavelet filter is designed with IFLF structure based on simple g_m-C integrator as basic block. Finally, the simulation results demonstrate the proposed approach is feasible and it also provides a relatively simple strategy for the WT implementation.

The paper is organized as follows. In section 2, Gaussian function and Gaussian wavelet series based on the multi-order derivatives of Gaussian function are analysis and proved as wavelet base. In Section 3, a general rational approximation model of Gaussian wavelet series in time domain is

described, which allows one to obtain a high accuracy approximated transfer function of wavelet system using QDE optimal algorithm. Section 4 illustrates a general design method of IFLF structure Gaussian wavelet filter with simple g_m-C integrator as basic building blocks. Theoretical approximation, circuit simulation and application analysis of the 5th order Gaussian wavelet filter are given in Section 5. Finally, Section 6 presents the conclusions.

2 | GAUSSIAN FUNCTION AND GAUSSIAN WAVELET SERIES

Gaussian wavelet is widely used to extract features of signals and images because of its good time-frequency local characteristics. Those Gaussian wavelets are constructed by the Gaussian function. The Gaussian function and its Fourier transform are given by

$$\psi_\sigma(t) = \frac{1}{\sqrt{2\pi}} e^{-t^2/(2\sigma^2)} \Rightarrow \Psi_\sigma(\omega) = e^{-\omega^2\sigma^2/2} \tag{1}$$

where σ is the scale factor of the Gaussian function. The characteristics of time and frequency domain of Gaussian function are shown in Figure 1.When σ=1, the 1st-6th order derivatives of Gaussian function are described as

$$\psi'(t) = \frac{-1}{\sqrt{2\pi}} t e^{-t^2/2} \tag{2}$$

$$\psi''(t) = \frac{-1}{\sqrt{2\pi}} (-t^2+1) e^{-t^2/2} \tag{3}$$

$$\psi'''(t) = \frac{-1}{\sqrt{2\pi}} (t^3-3t) e^{-t^2/2} \tag{4}$$

$$\psi^{(4)}(t) = \frac{-1}{\sqrt{2\pi}} (-t^4+6t^2-3) e^{-t^2/2} \tag{5}$$

$$\psi^{(5)}(t) = \frac{-1}{\sqrt{2\pi}} (t^5-10t^3+15t) e^{-t^2/2} \tag{6}$$

$$\psi^{(6)}(t) = \frac{-1}{\sqrt{2\pi}} (-t^6+15t^4-45t^2+15) e^{-t^2/2} \tag{7}$$

The corresponding functions of 1st-6th order derivatives of Gaussian are shown in Figure 2. From (2)-(7), we can find that every derivative has no uniform expression. However, in frequency domain, according to the higher order differential properties of Fourier transform in (8), the frequency function can be derived in (9).

$$F[f^{(n)}(t)] = (j\omega)^n F(\omega) \tag{8}$$

$$\Psi_\sigma^{(n)}(\omega) = (j\omega)^n e^{-\omega^2\sigma^2/2} \tag{9}$$

Now we should prove every derivative of Gaussian function satisfies the admissibility condition of wavelet base in (10) so that the original signal can be reconstructed by the inverse WT.

$$C_\Psi = \int_{-\infty}^{\infty} \frac{|\Psi(\omega)|^2}{|\omega|} d\omega < +\infty \tag{10}$$

Substituting (9) into (10), we get

$$C_\Psi = \int_{-\infty}^{\infty} \left| \omega^{2n-1} \cdot e^{-\sigma^2\omega^2} \right| d\omega \tag{11}$$

Applying L'Hopital's rule to prove the function in (11) is bounded and convergent, that is

$$\lim_{\omega\to\pm\infty}\omega^{2n-1}\cdot e^{-\sigma^2\omega^2}=\lim_{\omega\to\pm\infty}\frac{e^{-\sigma^2\omega^2}}{1/\omega^{2n-1}}=\frac{0}{0}=0 \tag{12}$$

Obviously, every derivative of Gaussian function satisfies the admissibility condition and they are the wavelet bases.

3 | RATIONAL APPROXIMATIONS OF GAUSSIAN WAVELET SERIES

3.1 | General approximation model of Gaussian wavelet series

The WT of a function $f(x)$ at the scale a and position b is defined by[25]

$$W_f(a,b)=\frac{1}{\sqrt{a}}\int_{-\infty}^{\infty}f(t)\psi^*(\frac{t-b}{a})dt \tag{13}$$

where $\psi(t)$ is wavelet base and * denotes the complex conjugation. According to signal and system theory, the analog computation of $W_f(a,b)$ can be achieved through the implementation of the linear filter bank of which the impulse response satisfies:

$$h(t)=\frac{1}{\sqrt{a}}\psi(\frac{-t}{a}) \tag{14}$$

Usually, for a given wavelet base $\psi(t)$ the transfer function $H(s)$ will be non-rational and non-causal. In order to obtain the Causality system, the wavelet base $\psi(t)$ must be time-reversed and time-shifted by a suitable value t_0. Therefore, the performance of the analog WT implementation depends firstly on the accuracy of the approximation to $\psi(t_0-t)$. For the generic situation of stable systems with distinct poles and conjugate complex poles, the impulse response function $h(t)$ is a linear combination of damped exponentials and exponentially damped harmonics. For low order systems, this makes it possible to propose an explicitly parameterized class of impulse response functions among which to search for a good approximation of the time-shifted wavelet $\psi(t_0-t)$. As an example, if a 5th order approximation of the aforementioned Gaussian wavelet is attempted, the functions model of $h(t)$ will typically be given as

$$h_{5th}(t)=k_1e^{k_2t}+2|k_3|e^{k_4t}\cos(k_5t+k_6)+2|k_7|e^{k_8t}\cos(k_9t+k_{10}) \tag{15}$$

where the parameters k_2, k_4 and k_8 must be strictly negative for reasons of stability. By modifying the approximation order, the corresponding items in the model can be increased or decreased. For instance, a 7th order approximation model of wavelet base is described as

$$h_{7th}(t)=k_1e^{k_2t}+2|k_3|e^{k_4t}\cos(k_5t+k_6)+2|k_7|e^{k_8t}\cos(k_9t+k_{10})+2|k_{11}|e^{k_{12}t}\cos(k_{13}t+k_{14}) \tag{16}$$

The squared L_2-norm based evaluation function between $h(t)$ and $\psi(t_0-t)$ is described as

$$\|h(t)-\psi(t_0-t)\|^2=\int_0^{+\infty}[h(t)-\psi(t_0-t)]^2dt \tag{17}$$

The explicit form in (17) can be minimized in some ways using numerical optimization techniques and software. When the choice of the time-shift is $t_0=3$, the mean squared error (MSE) of the discrete points is respectively given as

$$E_{MSE}(k)=\frac{1}{M}\sum_{n=1}^{M}[h(n\Delta t)-\psi(3-n\Delta t)]^2 \tag{18}$$

where M is the sampling points and Δt is the sampling time interval. To obtain a stable 5th order approximation $h(t)$ to $\psi(t_0-t)$, the optimization model for approximating the Gaussian wavelet series in time domain is defined as

$$\begin{cases} \min E_{MSE}(k) = \dfrac{1}{M}\sum_{n=1}^{M}[h(n\Delta t) - \psi(3 - n\Delta t)]^2 \\ s.t.\ k_2 < 0, k_4 < 0, k_8 < 0 \end{cases} \tag{19}$$

Next, the nonlinear constrained optimization problem in (19) will be solved using QDE algorithm.

3.2 | Approximating Gaussian wavelet series using QDE algorithm

(1) Encoding and measurement for quantum chromosome

In the quantum evolution computation, a *Q*-bit has two ground states: $|0\rangle$ and $|1\rangle$. According to the principle of superposition, a *Q*-bit may be in the "1" state, in the "0" state, or in a linear superposition of two states.

$$|\phi\rangle = \alpha|0\rangle + \beta|1\rangle \tag{20}$$

where α and β is the probability amplitude of $|0\rangle$ and $|1\rangle$ state, respectively, which satisfy the normalization condition $|\alpha|^2 + |\beta|^2 = 1$. In this algorithm, the probability amplitude of the *Q*-bit is described as $[\theta] = [\cos\theta \ \ \sin\theta]^T$ using quantum angle. For population scale *n* and length *d*, the quantum individual encoding is defined as

$$\boldsymbol{q}_i^t = \begin{bmatrix} \cos(\theta_1^t) & \cos(\theta_2^t) & \cdots & \cos(\theta_d^t) \\ \sin(\theta_1^t) & \sin(\theta_2^t) & \cdots & \sin(\theta_d^t) \end{bmatrix}, i = 1, 2, \cdots, n \tag{21}$$

Equation (21) can be simplified as $\boldsymbol{q}_i^t = (\theta_1^t, \theta_2^t, \cdots, \theta_d^t)$ using the quantum rotating angle. In population initialization, the individual quantum angles $\theta_l^t (l = 1, 2, \cdots d; t = 0)$ are randomly generated in $[0, 2\pi]$. In order to evaluate the goodness of the quantum individual, the *Q*-bit states of the individual need be measured by collapsing the superposition states into classical bit states. The measurement method of the quantum individual is described as follows. A random number $r \in [0,1]$ is generated. If $r > \left|\cos(\theta_l^t)\right|^2$, then the value of this bit is 1, otherwise it is 0. So a quantum chromosome will become a binary string by this method and we can use the binary string to solve the problem required.

(2) Quantum chromosome updating by differential evolution

The differential evolution (DE) is a kind of population based stochastic optimization algorithm proposed by Storn and Price[26]. The DE adopts the real number encoding scheme, mutation, crossover and selection operation based on differential vectors. In this work, the DE is used to update the quantum chromosome[27] by employing its excellent ability of overall search ability.

According to the encoding regulation of quantum chromosome, which we have discussed above, we encode the quantum individual $\boldsymbol{q}_i^t = (\theta_1^t, \theta_2^t, \cdots, \theta_d^t)$, where *d* is the length of chromosome.

Suppose $\boldsymbol{v}_i^t$ is the corresponding individual obtained by practicing the mutation operator on individual $\boldsymbol{q}_i^t$. The selected mutation operator is

$$\boldsymbol{v}_i^t = \boldsymbol{q}_i^t + F \cdot [(\boldsymbol{q}_{best}^t - \boldsymbol{q}_i^t) + (\boldsymbol{q}_{r1}^t - \boldsymbol{q}_{r2}^t)] \tag{22}$$

where $r_1, r_2 \in [1, n]$, they are different from each other and different from *i*. $\boldsymbol{q}_{best}^t$ is the best individual in the current generation. $F \in (0,1)$ is the mutation factor which controls the amplification of the differential variation.

In order to increase the diversity of the parameter vector, the crossover operator is applied on the up-level individuals of the population. A trial vector $\boldsymbol{u}_i^t$ is generated with

$$u_{ij}^t = \begin{cases} \upsilon_{ij}^t, rand(\cdot) \le CR \,|\, j = rand\ n \\ \theta_{ij}^t, others \end{cases} \tag{23}$$

where $rand(\cdot) \in [0,1]$ is a uniform random number. $CR \in [0,1]$ is the crossover probability constant. $rand\ n \in [1, d]$ is a randomly chosen index, and θ_{ij}^t is the *j*th quantum angle of the individual $\boldsymbol{q}_i^t$. Finally, a selection operator based on greedy algorithm is applied to compare the fitness function values of two competing vectors. The better individual will survive the next generation.

$$\boldsymbol{q}_i^{t+1} = \begin{cases} \boldsymbol{u}_i^t, f\left(\boldsymbol{u}_i^t\right) \le f\left(\boldsymbol{q}_i^t\right) \\ \boldsymbol{q}_i^t, otherwise \end{cases} \tag{24}$$

where f denotes the fitness function in (19).

(3) QDE for Gaussian wavelet series approximation

The proposed QDE algorithm is used to solve the nonlinear constrained optimization problem in (19) for approximating Gaussian wavelet series. The processing procedure of QDE is as follows:

*Step*1: Initialize control parameters. Specify the population size P_n=10, the sampling time interval $\Delta t = 0.01$, the number of the sampling points *M*=900, the maximum evolution generation *T*=4900, the step of the quantum rotating angle is 0.01π. Set the value of the control parameters for QDE, difference vector scale factor *F*=0.85, crossover probability constant *CR*=0.7.

*Step*2: Initialize the population. Determine initial population $\boldsymbol{p}^0 = [\boldsymbol{q}_1^0; \boldsymbol{q}_2^0; \cdots; \boldsymbol{q}_n^0]$, where $\boldsymbol{q}_i^o = (\theta_1^0, \theta_2^0, \cdots, \theta_d^0)$, *n* is the population scale and *d* is the length of chromosome.

*Step*3: Evaluate the individual. Obtain the fitness values of the individual, store the best one into $\boldsymbol{q}_{best}$.

*Step*4: Updating the quantum individual. Update the quantum chromosome by QDE strategy and produce the next generation quantum individual.

*Step*5: Evaluate the fitness of the quantum chromosome and store the optimum individual $\boldsymbol{q}_{best}^{t}$ in this generation. If $\boldsymbol{q}_{best}^{t}$ is superior to $\boldsymbol{q}_{best}$, then $\boldsymbol{q}_{best}^{t} \to \boldsymbol{q}_{best}$; Otherwise $\boldsymbol{q}_{best} \to \boldsymbol{q}_{best}^{t}$. After this operation, we save the better individual for the next generation iteration.

*Step*6: Stopping condition check. If the evolution generation $t \le T$ is met or the optimum results are found, output the optimum; else set $t \leftarrow t+1$, return to Step 4 until to the maximum number of generation.

According to the above steps of the QDE algorithm, the accurate global optimal solution k_i of the 5th order approximation $h(t)$ is obtained in Table 1. The transfer functions of first order derivative of Gaussian wavelet filter (scale σ=1) resulting from this approximation is obtained as

$$H(s) = \frac{0.0127s^4 - 0.2889s^3 + 0.6301s^2 - 2.5699s + 0.0553}{s^5 + 2.3654s^4 + 7.1894s^3 + 8.0957s^2 + 7.5910s + 2.2355} \tag{25}$$

The approximated Gaussian wavelets using the improved Maclaurin method[17], L_2, DE and QDE algorithms are shown in Figure 3. Among them, because the improved Maclaurin method[17] is a frequency domain method, so the approximation result needs to be transformed into the time domain. The approximation MSE based on different algorithms is shown in Table 2. From the comparisons, the QDE algorithm is more accurate than the improved Maclaurin method[17], DE and L_2 algorithms. Compared with the QDE and DE algorithm, L_2 algorithm has the simplest computation process. However, one disadvantage of the L_2 algorithm is that the computational accuracy is affected by the initial value so that it is difficult to select the initial value of the optimal solution. Obviously, the improved Maclaurin method[17] has the lowest time domain approximation accuracy because it only approximates the denominator of the transfer function in frequency domain. The main advantage of this algorithm is that the numerator of the obtained transfer function has only one term, and the feed-forward path in the multi-loop feedback network will be relatively simple. On account of the proposed approximation model is based on the linear system theory, the research shows that the constructed general model can be used to approximate arbitrarily wavelet function based on desired accuracy. Furthermore, because the model approximation is based on the numerical solution, it is also suitable for the wavelet bases without explicit expression such as Daubechies (Db) wavelet.

The approximation coefficients of 2nd-3rd order derivative of Gaussian wavelet using the 5th order approximation model are also listed in Table 1. The associated approximation functions are shown in Figure 4 (A)-(C). The approximation coefficients of 4th-6th order derivative of Gaussian wavelet based on the 7th order approximation model are listed in Table 3. The associated approximated wavelet bases are shown in Figure 4 (D)-(F). From these simulation results, we can see that the proposed approximation model and solution algorithm in this work can get a better rational approximation function of Gaussian wavelet series. Next, three main parameters (i.e. approximation order N, sampling interval Δt and time-shifted t_0) affecting the approximation accuracy of wavelet function are further discussed. To higher order N, it is well known that the approximation accuracy of wavelet base will be higher. However, the associated analog network will be more complex. If the value of the sampling interval Δt goes down, the approximation precision becomes better but it will spend more time to compute. Karel et al[11] and Zhao et al[28] have shown that different values of time-shifted t_0 affect the approximation accuracy. However, there is no comprehensive analysis combined with the other two factors. On the one hand, t_0 shifting too much may make the beginning of the wavelet have a relatively flat slope, which leads to the need

for high order (N) approximation model to achieve high precision. On the other hand, shifting too little yields truncation of wavelet base and causes an integral not to be zero, which makes it difficult to restore the wavelet. Commonly, the time-shifted t_0 should be chosen reasonably according to the approximate support regions of the wavelet. In the next section, the obtained approximation function of wavelet base will be employed to design analog wavelet filter.

4 | GENERAL DESIGN METHOD OF GAUSSIAN WAVELET FILTER

From the system theory we know that there are many possible state space descriptions for a circuit that implements a certain transfer function, since state-space descriptions and their corresponding filter topologies are not unique representations of a dynamical system. Hence, the designer is allowed to find a circuit that fits his/her specific requirements. The trend towards low power integrated continuous-time filters has increased the interest in new design techniques for analog integrated filters[29, 30]. In this work, the g_m-C integrator and the IFLF structure are used to implement wavelet filter. The 5th order general transfer function of wavelet filter can be described as

$$H(s)=\frac{A_4s^4+A_3s^3+A_2s^2+A_1s+A_0}{B_5s^5+B_4s^4+B_3s^3+B_2s^2+B_1s+B_0} \tag{26}$$

As an example, the first order derivative of Gaussian wavelet is selected. A similar procedure can also be applied for other wavelet filter implementations. The approximated 5th order transfer function of first order derivative of Gaussian wavelet filter can be realized by the IFLF topology[31-33] depicted in Figure 5. The realized general transfer function is given by

$$H(s)=\frac{\frac{G_4}{\tau_1}s^4+\frac{G_3}{\tau_1\tau_2}s^3+\frac{G_2}{\tau_1\tau_2\tau_3}s^2+\frac{G_1}{\tau_1\tau_2\tau_3\tau_4}s+\frac{G_0}{\tau_1\tau_2\tau_3\tau_4\tau_5}}{s^5+\frac{1}{\tau_1}s^4+\frac{1}{\tau_1\tau_2}s^3+\frac{1}{\tau_1\tau_2\tau_3}s^2+\frac{1}{\tau_1\tau_2\tau_3\tau_4}s+\frac{1}{\tau_1\tau_2\tau_3\tau_4\tau_5}} \tag{27}$$

where τ_i is the time constant and G_j is the gain factor. Comparing (26) with (27) the derived expressions of τ_i and G_j are described as

$$\tau_i=\tau\left(\frac{B_{5-i+1}}{B_{5-i}}\right)(i=1,2,\cdots 5)\ ,\quad G_j=\frac{A_j}{B_j}(j=0,1,\cdots 4) \tag{28}$$

where $\tau=1/\omega_u$, ω_u is the unity-gain frequency.

The simple OTA used as the active element in the integrators of Figure 5 is given in Figure 6. Considering that the MOS transistors operate in subthreshold region, the transistors Mn5-Mn6 and Mn7-Mn8 have aspect rations A:1 and 1:A, respectively. The value of the transconductance of the OTA is given by[34, 35]

$$g_m=\frac{I_o}{kV_T}\frac{4A}{(1+A)^2} \tag{29}$$

where V_T is the thermal voltage, k is the subthreshold slope factor of an MOS transistor and I_o is the bias current. The realized time constants of (27) are given by

$$\tau_i=\frac{C_i}{g_m}=\frac{C_ikV_T}{I_o}\frac{(1+A)^2}{4A},i=1,2,\cdots,n \tag{30}$$

Setting A=5 and according to (25) and (28), it is easy to obtain the time-constant τ_i and gain factors G_j. Using simple g_m-C integrator as the basic block, the designed 5th order Gaussian filter circuit is

shown in Figure 7. Next, the performance of the designed generalized filter structure will be evaluated through circuit simulation.

5 | SIMULATIONS AND ANALYSIS

The designed first order derivative of Gaussian wavelet filter in a 0.35μm CMOS process was simulated using PSpice software. The supply voltage was V_{DD}=0.53V and V_{SS}=-0.53V. The aspect rations of the transistors of the OTA are 10μm/2.5μm for M_9-M_{10}, 25μm/5μm for M5, M8, 5μm/5μm for M6, M7 and 60μm/1.5μm for M1-M3. The calculated values of capacitor C_i and gain factors G_j are summarized in Table 4 when the bias current I_o is set to 2.5*n*A. Because the five order term in the numerator of the transfer function is equal to 0, so G_5 is 0. In addition, the minus sign in G_1 and G_3, corresponding to the circuit diagram, means the input signal is connected to the reverse input terminal of the OTA.

The simulated and QDE approximated impulse responses of the wavelet filter are shown in Figure 8. The excellent approximation for the approximated first order derivative of Gaussian wavelet based on QDE algorithm confirms the performance of the design wavelet circuit. In order to verify the performance of the whole wavelet filter system, which is able to scale and shift the wavelet base function, another simulation is operated in the next. By changing the values of the bias currents in the g_m-C integrator of the designed wavelet filter circuit, which can obtain a dyadic scale system, other different scales (σ=0.5, 2) first order derivative of Gaussian wavelets are illustrated in Figure 9. The output results also have good approximation performance. Alternatively, we may change the capacitance values (C_i) to get the same results. Figure 10 illustrates the frequency responses of the wavelet filter circuit and the approximated wavelet system for 3 dyadic scales (σ=0.5, 1, 2). We can see that the simulation value of the wavelet filter circuit is close to the approximation value. By denormalizing the filter transfer function, the center frequency of the filter can be moved to the desired frequency point. Because the MOSFETS are susceptible to temperature changes, therefore in order to demonstrate the stability of the designed circuit, the temperature sweep analysis using Monte Carlo analysis is performed for temperature variations from 0-50°C with 1°C increment. The wavelet circuit output result (σ=1) is shown in Figure 11, which shows the small variation with temperature. The origin of this phenomenon is that the MOSFETS in the weak inversion operation are affected by the thermal voltage. Finally, the performance of the designed wavelet filter is summarized in Table 5. The root-mean-square values of the input- referred noise can be obtained by the noise integrated within the passband of each filter as 0.0188V, 0.0266V and 0.0334V, respectively. Thus, the dynamic range of the filter with different scales is about 29 dB, 26 dB and 24 dB, respectively. However, the circuit has a relatively low dynamic range. The main reason is that the maximum input signal is limited to linear range of the circuit, and the minimum range of acceptable input signal is limited to noise level.

Furthermore, in order to evaluate the performance of the proposed general method in the application, the multi-scale wavelet filters are applied to the front-end signal processing of QRS detection in ECG signal. The wavelet filter output signals will be analyzed by the QRS detection algorithm in Cui et al[36]. The block diagram of QRS detection based on wavelet filter is shown in Figure 12. The four wavelet filters with different scales $\sigma=2^1, 2^2, 2^3, 2^4$ are used to preprocess ECG signal. The main strategy of the detection algorithm reported in Cui et al[36] is to first determine the position of R-wave using the modulus maxima method, and then determine Q-wave and S-wave based on modulus maximum lines. The ECG signals (ECG 100 and 105) in the MIT-BIH database

is used as the input signal of the detection system. ECG 100 is a pure signal and ECG 105 is a natural ECG signal with baseline drift and much noise. The output signals of the wavelet filters with four scales are shown in Figure 13 and 14, respectively. Figure 13 and 14 show that the transformed signal can better locate the peak point of QRS after passing the wavelet filters. In order to further verify the validity of the wavelet filter in QRS detection, the detection results of the selected nine ECG signals are shown in Table 6. The accuracy detection rate of the QRS detection based on multi-scale wavelet filters is 96.86 % (false detection rate 3.14%), which is close to the results of the method in Cui et al[36]. The obvious reason is that the method in Cui et al[36] uses complete digital analysis, which has a higher detection accuracy than the detection method based on wavelet filter circuit. The application results indicate the proposed general method is feasible for wavelet filter design.

6 | CONCLUSION

To implement WT in analog domain, high accuracy general rational approximation model of Gaussian wavelet series in time domain is built and wavelet filter circuit is designed using continuous-time analog circuit with multiple loop feedback structure, which is composed with g_m-C integrators as the basic building blocks. The proposed approximation model of wavelet base may be extended to arbitrarily order and any wavelet function including the wavelet base without explicit formulation. Taking the first order derivative of Gaussian wavelet base as an example, the 5th order rational approximation model is applied to obtain the approximated transfer function of wavelet filter. The approximation results indicate the proposed time domain approximation method is superior to the DE, L_2 and improved Maclaurin approach. Then the IFLF structure first order derivative of Gaussian wavelet filter is designed using simple g_m-C integrators as the basic blocks. By adjusting the bias current of the OTA, different scale wavelet function can be easily obtained for the WT implementation. The simulation and practical application results of wavelet filter circuit demonstrate the design method is effective. Furthermore, this method also provides a general way for other analog WT implementation based on different wavelet base.

REFERENCES

1. Debnath L, Shah F A. Wavelet Transforms and Their Applications. London: Birkhäuser, 2015.
2. Daubechies I. The wavelet transform, time-frequency localization and signal analysis. *IEEE Transactions on Information Theory*. 1990; 36(5):961-1005,.
3. Haddad S A P, Serdijn W A. Ultra Low-Power Biomedical Signal Processing: An Analog Wavelet Filter Approach for Pacemakers. Berlin: Springer, 2009.
4. Karel J M H, Haddad S A P, Hiseni S, Westra R L, Serdijn W A, Peeters R L M. Implementing wavelets in continuous-time analog circuits with dynamic range optimization. *IEEE Transactions on Circuits and Systems*. 2012; 59(2):229-242.
5. Haddad S A P, Sumit B, Serdijn W A. Log-domain wavelet bases. *IEEE Transactions on Circuits and Systems*. 2005; 52(10):2023-2032.
6. Casson A J, E Rodriguez-Villegas. A 60pW g_m-C continuous wavelet transform circuit for portable EEG systems. *IEEE Journal of Solid-State Circuits*. 2011; 46(6):1406-1415.
7. Güler I, Übeyli E D. Adaptive neuro-fuzzy inference system for classification of EEG signals using wavelet coefficients. *Journal of Neuroscience Methods*. 2005; 148(2): 113-121.

8. Hazarika N, Chen J Z, Tsoi A C, Sergejew A. Classification of EEG signals using the wavelet transform. *Proc. 13th International Conference on Digital Signal Processing*. 1997; 89-92.
9. Chaniyara P M, Srivastava P K, Suresha B, Reddy A S. Design of sampled analog wavelet processor architecture for cochlear implant application. *Analog Integrated Circuits and Signal Processing*. 2016; 86(2): 171-180.
10. Gopalakrishna V, Kehtarnavaz N, Loizou P C. A recursive wavelet-based strategy for real-time cochlear implant speech processing on PDA platforms. *IEEE Transactions on Biomedical Engineering*. 2010; 57(8): 2053-2063.
11. Karel J M H, Peeters R L M, Wetra R L, Haddad S A P, Serdijn W A. An L_2-based approach for wavelet approximation. *Proc. IEEE Conference on Decision and Control and European Control Conference*. 2005; 7882-7887.
12. Li H M, He Y G, Sun Y. Detection of cardiac signal characteristic point using log-domain wavelet transform circuits. *Circuits, Systems and Signal Processing*. 2008; 27(5):683–698.
13. Li M, He Y. Analog VLSI implementation of wavelet transform using switched-current circuits. *Analog Integrated Circuits and Signal Processing*. 2012; 71(2):283-291.
14. Li M, He Y. Analog wavelet transform using multiple-loop feedback switched-current filters and simulated annealing algorithms. *AEÜ-International Journal of Electronics and Communications*. 2014; 68(5):388-394.
15. Zhao W, Sun Y, He Y. Minimum component high frequency Gm-C wavelet filters based on Maclaurin series and multiple loop feedback. *Electronic Letters*. 2010; 46(1): 34-36.
16. Diab M S, Mahmoud S A. A 6nw seventh-order OTA-C band pass filter for continuous wavelet transform. *Proc. International SoC Design Conference*. 2009; 196-197.
17. Zhao W, Ma L, Zhang Y, He Y, Sun Y. Realization of analog wavelet filter using hybrid genetic algorithm for on-line Epileptic event detection. *IEEE Access*. 2020; 8: 33137-33150.
18. Lin J, Ki W H, Edwards T, Shamma S. Analog VLSI implementations of auditory wavelet transforms using switched-capacitor circuits. *IEEE Transactions on Circuits and Systems*. 1994; 41(9):572-583.
19. Laoudias C, Beis C, Psychalinos C. 0.5V wavelet filters using current mirrors. *Proc. IEEE International Symposium of Circuits and Systems*. 2011; 1443-1446.
20. Sedra A S, Roberts G W, Gohh F. The current conveyor: history, progress and new results. *IEE Proceedings G-Circuits, Devices and Systems*. 1990; 137(2): 78-87.
21. Chen Y, Mak P I, Zhou Y. Source-follower-based bi-quad cell for continuous-time zero-pole type filters. *Proc. IEEE International Symposium on Circuits and Systems*. 2010; 3629-3632.
22. Chen Y, Mak P I, Zhang L, He Q, Wang Y. 0.013 mm2, kHz-to-GHz-bandwidth, third order all-pole lowpass filter with 0.52-to-1.11 pW/pole/Hz efficiency. *Electronics Letters*, 2013; 49(21):1340-1342.
23. Chen Y, Zhou Y. A low power CMOS mixed-integrator-based continuous-time filter. *Proc. IEEE 8th International Conference on ASIC*. 2009; 274-276.
24. Chen Y, Mak P I, Zhou Y. Mixed-integrator biquad for continuous-time filters. *Electronics Letters*, 2010; 46(8):56-563.
25. Meshkat A, Dehghani R. A new discrete wavelet transform appropriate for hardware implementation. *International Journal of Circuit Theory and Applications*. 2020; 48(3):369-384.
26. Storn R, Price K. Differential evolution-a simple and efficient heuristic for global optimization over continuous spaces. *Journal of Global Optimization*, 1997; 11:341-359.
27. Zheng T, Yamashiro M. Solving flow shop scheduling problems by quantum differential evolutionary algorithm. *International Journal of Advanced Manufacturing Technology*. 2010; 49(5): 643-662.
28. Zhao W, He Y. Realization of wavelet transform using switched-current filters. *Analog Integrated Circuits and*

Signal Processing. 2012; 71(2): 571-581.

29. Liu H, Zhu X, Lu M, Sun Y, Yeo K S. Design of reconfigurable dB-linear variable-gain amplifier and switchable-order g_m-C filter in 65-nm CMOS technology. *IEEE Transactions on Microwave Theory and Techniques*. 2019; 67(12):5148-5158.
30. Krishna J R M, Laxminidhi T. Widely tunable low-pass g_m–C filter for biomedical applications. *IET Circuits, Devices and Systems*. 2019; 13(2):239-244.
31. Sun Y, Fidler J K. Synthesis and performance analysis of universal minimum component integrator-based IFLF OTA-grounded capacitor filter. *IEE Proceedings: Circuits, Devices and Systems*. 1996; 143(2):107-114.
32. Hasan M, Zhu Y Q, Sun Y. Design for testability of high-order OTA-C filters. *International Journal of Circuit Theory and Applications*. 2016; 44(10):1859-1873.
33. Sun Y, Zhu X, Moritz J. Explicit design formulas for current-mode leap-frog OTA-C filters and 300 MHz CMOS seventh-order linear phase filter. *International Journal of Circuit Theory and Applications*. 2010; 38(4):367-382.
34. Corbishley P, Rodriguez-Villegas E. A nanopower bandpass filter for detection of an acoustic signal in a wearable breathing detector. *IEEE Transactions on Biomedical Circuits and Systems*. 2007; 1(3):163-171.
35. Tsirimokou G, Psychalinos C, Elwakil A S, Salama K N. Electronically tunable fully integrated fractional-order resonator. *IEEE Transactions on Circuits and Systems*. 2018; 65(2):166-170.
36. Li C W, Zheng C X, Tai C F. Detection of ECG characteristic points using wavelet transforms. *IEEE Transactions on Biomedical Engineering*, 1995; 42(1):21-28.

TABLE 1 The 5th order approximation coefficients of 1st-3rd order derivative of Gaussian wavelet

Approximated coefficients	$\Psi'(t)$	$\Psi''(t)$	$\Psi'''(t)$

k_1	0.313	-0.241	0.651
k_2	-0.421	-0.648	-1.809
k_3	-0.533	0.226	-0.230
k_4	-0.510	-0.181	-0.166
k_5	1.010	-1.205	2.416
k_6	-4.620	7.895	-83.754
k_7	0.213	0.127	-0.341
k_8	-0.462	-0.144	-0.178
k_9	-1.983	2.151	1.470
k_{10}	-4.216	0.559	2.106

TABLE 2 Comparison of approximation mean squared error (MSE) of different methods

Methods	Improved Maclaurin method[17]	L_2	DE	QDE
Approximation order	5	5	5	5
MSE	6.916×10^{-4}	1.292×10^{-4}	9.803×10^{-5}	3.496×10^{-5}

TABLE 3 The 7th order approximation coefficients of 4th-6th derivative of Gaussian wavelet

Approximated coefficients	$\Psi^{(4)}(t)$	$\Psi^{(5)}(t)$	$\Psi^{(6)}(t)$
k_1	0.879	1.124	-3.779
k_2	-1.518	-1.384	-1.602
k_3	0.868	-1.779	-5.519
k_4	-0.262	-0.240	-0.308
k_5	-2.277	2.207	-2.475
k_6	2.970	2.162	0.528
k_7	0.623	-0.808	2.950
k_8	-0.257	-0.204	-0.330
k_9	-1.391	3.114	1.627
k_{10}	-7.401	4.438	3.563
k_{11}	0.261	0.742	2.233
k_{12}	-0.238	-0.247	-0.260
k_{13}	-3.209	1.317	3.363
k_{14}	-5.493	-6.249	-4.531

TABLE 4 Capacitor and gain factor of Gaussian wavelet filter

Bias current and capacitor	Value	Gain factor	Value
I_o	2.500nA	G_0	0.025
C_1	23.972pF	G_1	-0.339

C_2	18.656pF	G_2	0.078
C_3	50.359pF	G_3	-0.040
C_4	60.475pF	G_4	0.005
C_5	192.549pF	G_5	0.000

TABLE 5 Performance of 3 scales wavelet filter circuits

Parameters	Values of performance		
Bias current (I_o)	I_o=5.0nA	I_o=2.5nA	I_o=1.25nA
Scale of wavelet (σ)	0.5	1	2
Transconductance (g_m)	71.22 nS	35.61nS	17.81 nS
Supply voltage	0.53V	0.53V	0.53V
Dynamic range (DR)	29 dB	26 dB	24 dB
Power dissipation	85.3nW	41.1nW	22.5 nW

TABLE 6 QRS detection results based on wavelet filter with four scales

ECG record name	Total beats	False positives	False negatives	Failed detection	False detection rate (%)	False detection rate by Cui et al[36] (%)
100	2273	0	1	1	0.044	0.000
101	1865	1	1	2	0.107	0.000
103	2084	1	0	1	0.048	0.000
105	2572	36	21	57	2.216	1.090
118	2278	1	0	1	0.044	0.040
119	1987	1	0	1	0.050	0.050
202	2136	0	2	2	0.094	0.050
207	1862	3	7	10	0.537	0.270
213	3251	0	0	0	0.000	0.000
Total	20308	43	32	75	3.140	1.500

FIGURE 1 Gaussian function. (A) Time domain (σ=1), (B) Frequency domain (σ=0.5)

FIGURE 2 Multi-order derivatives of Gaussian function. (A) 1st order derivative, (B) 2nd order derivative, (C) 3rd order derivative, (D) 4th order derivative, (E) 5th order derivative, (F) 6th order derivative

FIGURE 3 First order derivative of Gaussian wavelet approximation with different algorithms (σ=1, t_0=3)

FIGURE 4 Time-reversed and time-shifted 2st-6th order derivative of Gaussian wavelet approximation (t_0=4). (A) 2nd order derivative (5th order model), (B) 3rd order derivative (5th order model), (C) 4th order derivative (7th order model), (D) 5th order derivative (7th order model), (E) 6th order derivative (7th order model)

FIGURE 5 Block diagram of the IFLF structure for wavelet filter

FIGURE 6 Simple operational transconductance amplifier (OTA)

FIGURE 7 5th order Gaussian wavelet filter using g_m-C integrators

FIGURE 8 Simulated and QDE approximated first order derivative of Gaussian wavelet (σ=1)

FIGURE 9 Simulated and approximated impulse responses of first order derivative of Gaussian wavelet with other scales (σ=0.5, 2)

FIGURE 10 Simulated and approximated frequency responses of first order derivative of Gaussian wavelet filter (σ=0.5, 1, 2)

FIGURE 11 Temperature sweep analysis of the designed wavelet circuit (σ=1)

FIGURE 12 Block diagram of QRS detection based on wavelet filters

FIGURE 13 ECG 100 signal and the outputs of wavelet filters with four scales

FIGURE 14 ECG 105 signal with baseline drift and much noise, and the outputs of wavelet filters with four scales

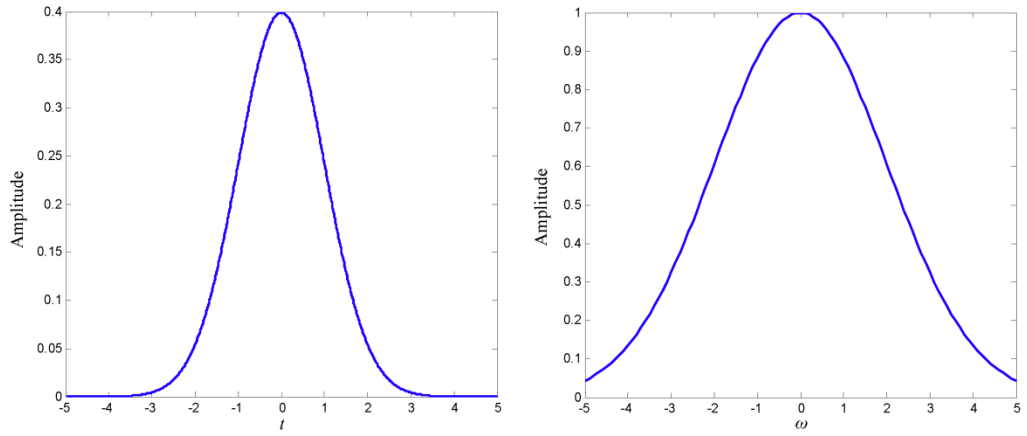

(A) (B)

FIGURE 1 Gaussian function. (A) Time domain (σ=1), (B) Frequency domain (σ=0.5)

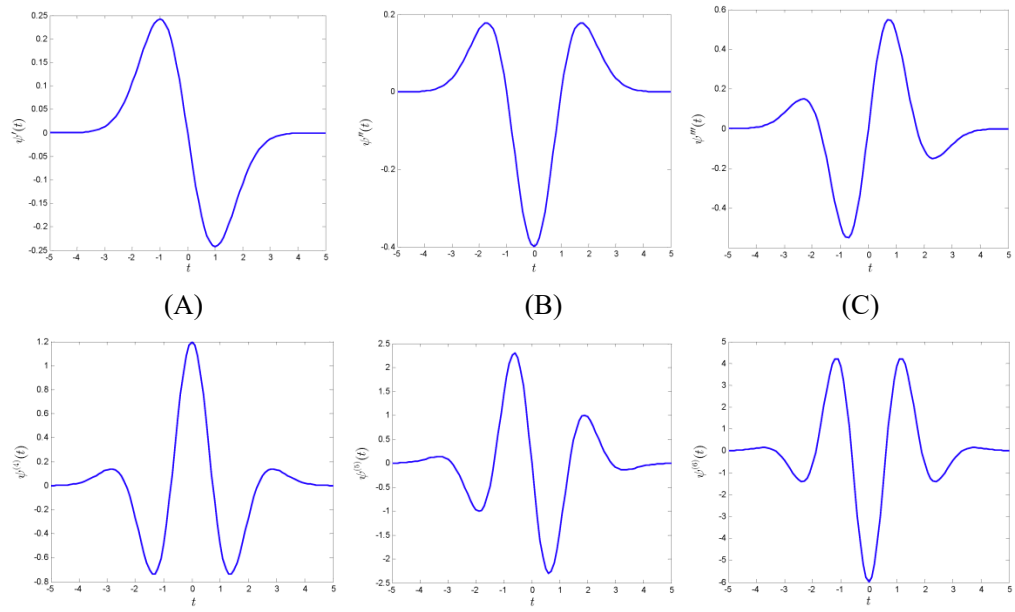

(A) (B) (C)

(D) (E) (F)

FIGURE 2 Multi-order derivatives of Gaussian function. (A) 1st order derivative, (B) 2nd order derivative, (C) 3rd order derivative, (D) 4th order derivative, (E) 5th order derivative, (F) 6th order derivative

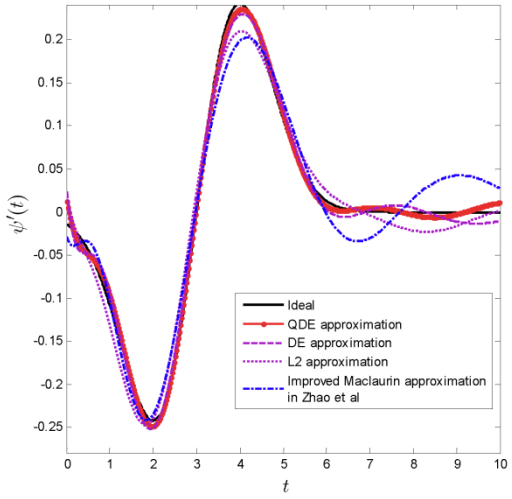

FIGURE 3 First order derivative of Gaussian wavelet approximation with different algorithms (σ=1, t_0=3)

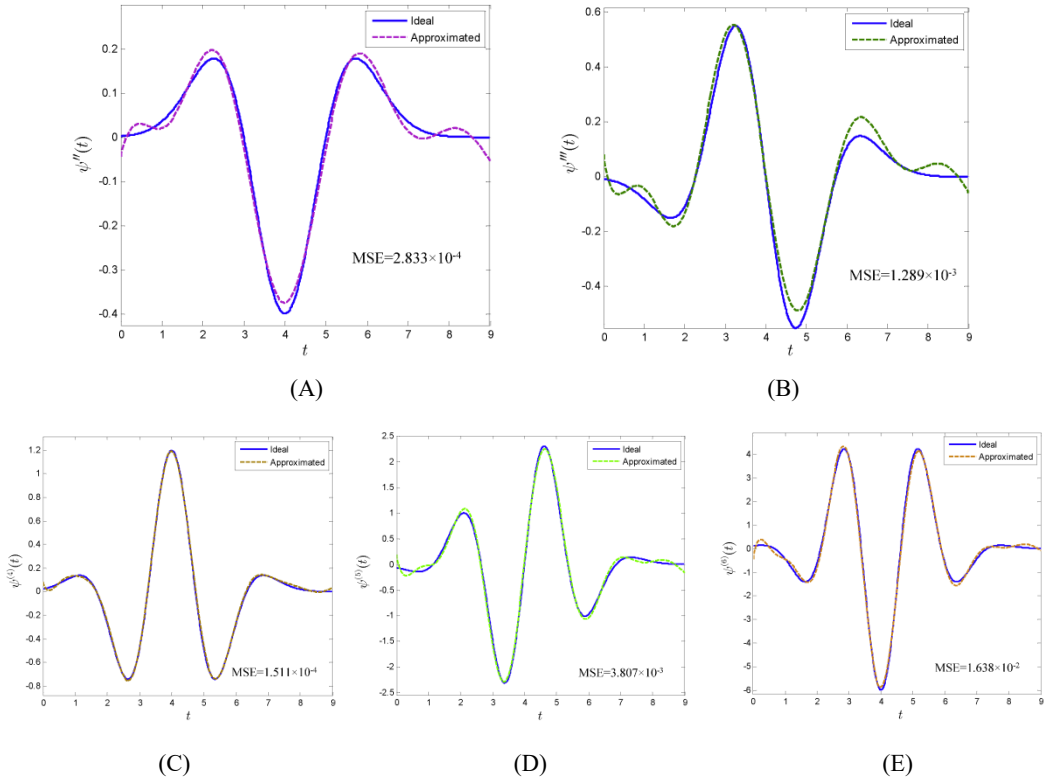

FIGURE 4 Time-reversed and time-shifted 2st-6th order derivative of Gaussian wavelet approximation (t_0=4). (A) 2nd order derivative (5th order model), (B) 3rd order derivative (5th order model), (C) 4th order derivative (7th order model), (D) 5th order derivative (7th order model), (E) 6th order derivative (7th order model)

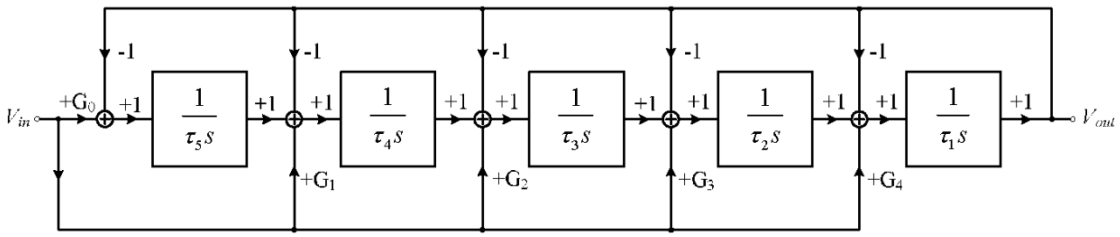

FIGURE 5 Block diagram of the IFLF structure for wavelet filter

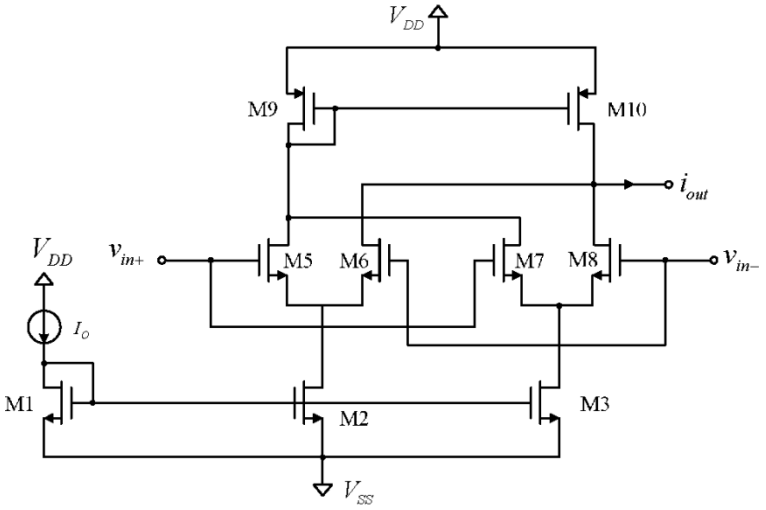

FIGURE 6 Simple operational transconductance amplifier (OTA)

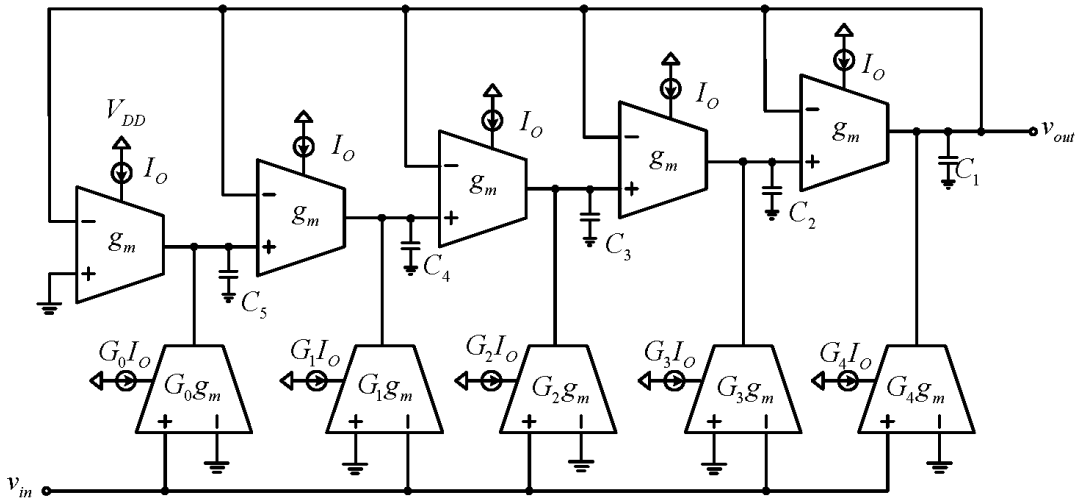

FIGURE 7 5th order Gaussian wavelet filter using g_m-C integrators

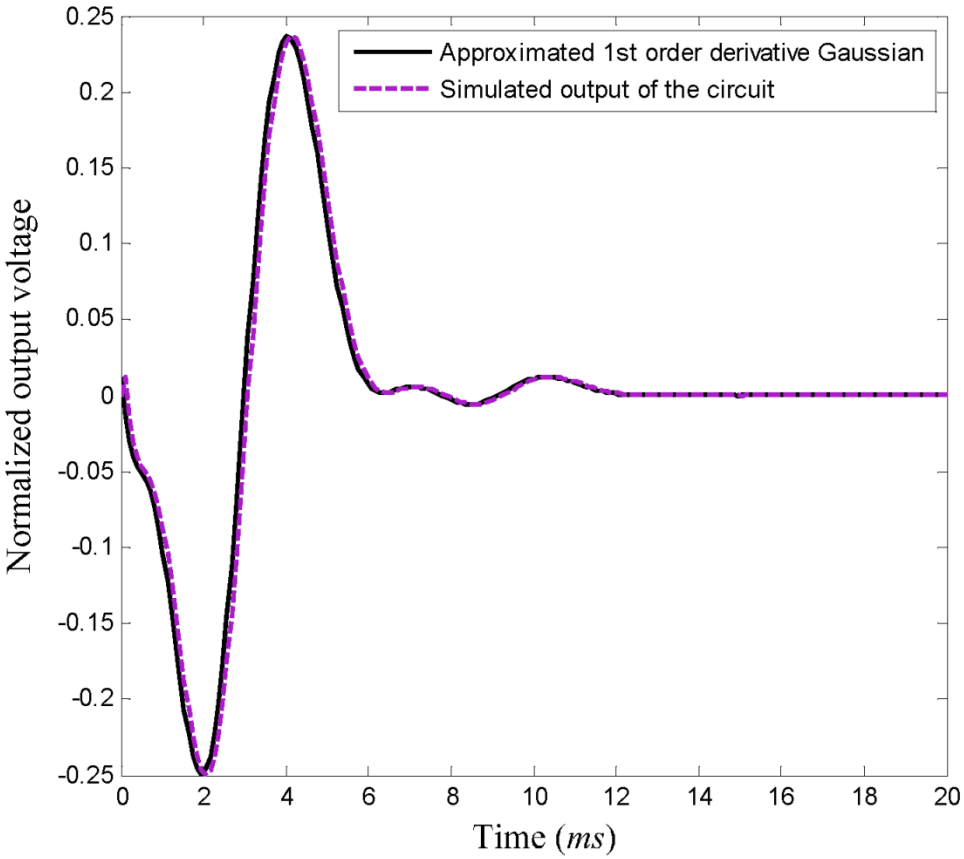

FIGURE 8 Simulated and QDE approximated first order derivative of Gaussian wavelet (σ=1)

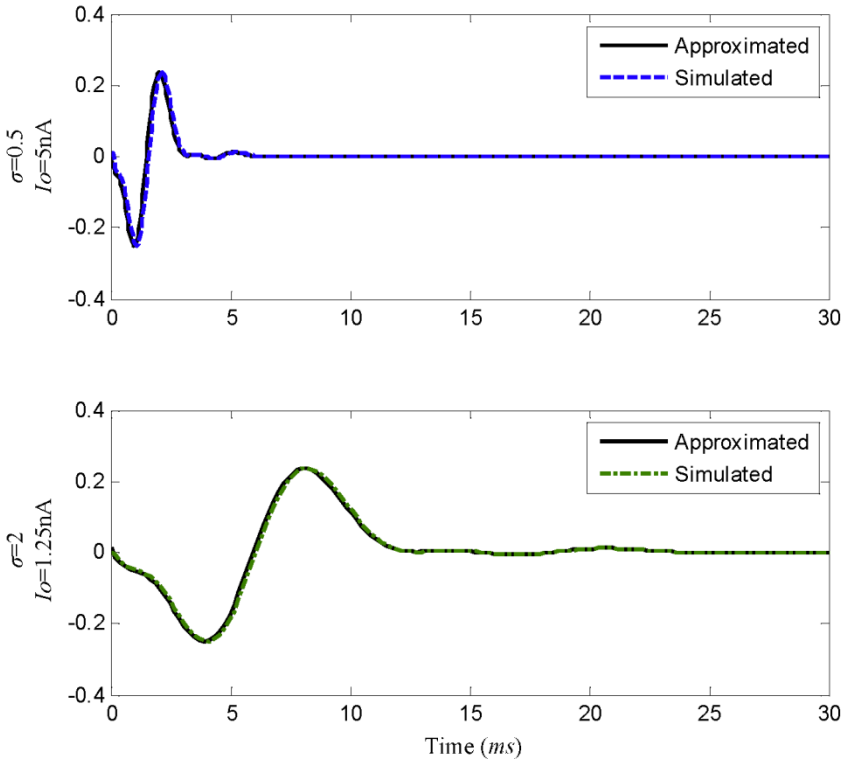

FIGURE 9 Simulated and approximated impulse responses of first order derivative of Gaussian wavelet with other scales (σ=0.5, 2)

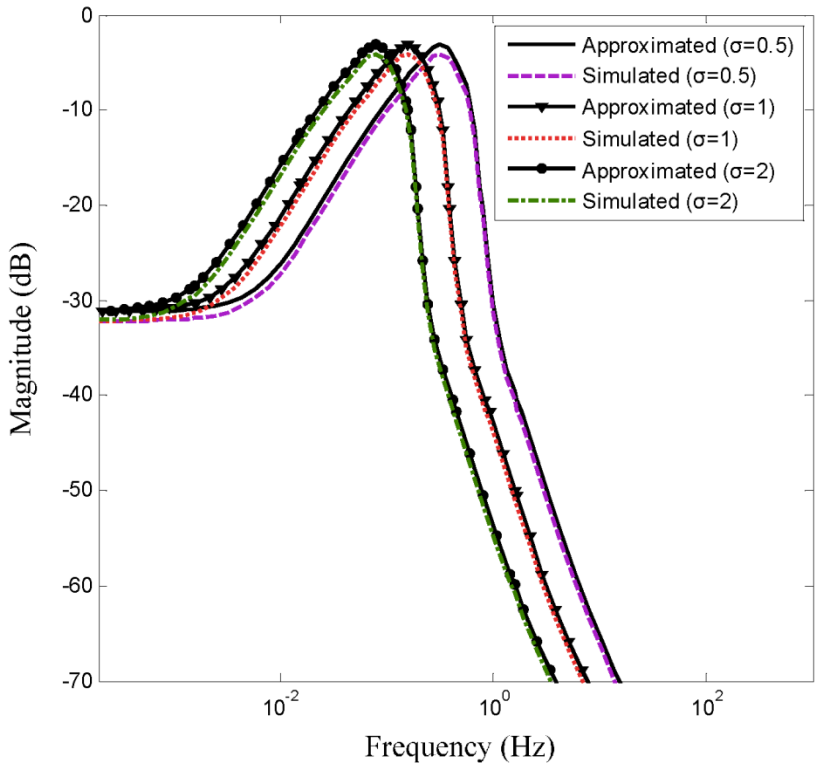

FIGURE 10 Simulated and approximated frequency responses of first order derivative of Gaussian wavelet filter (σ=0.5, 1, 2)

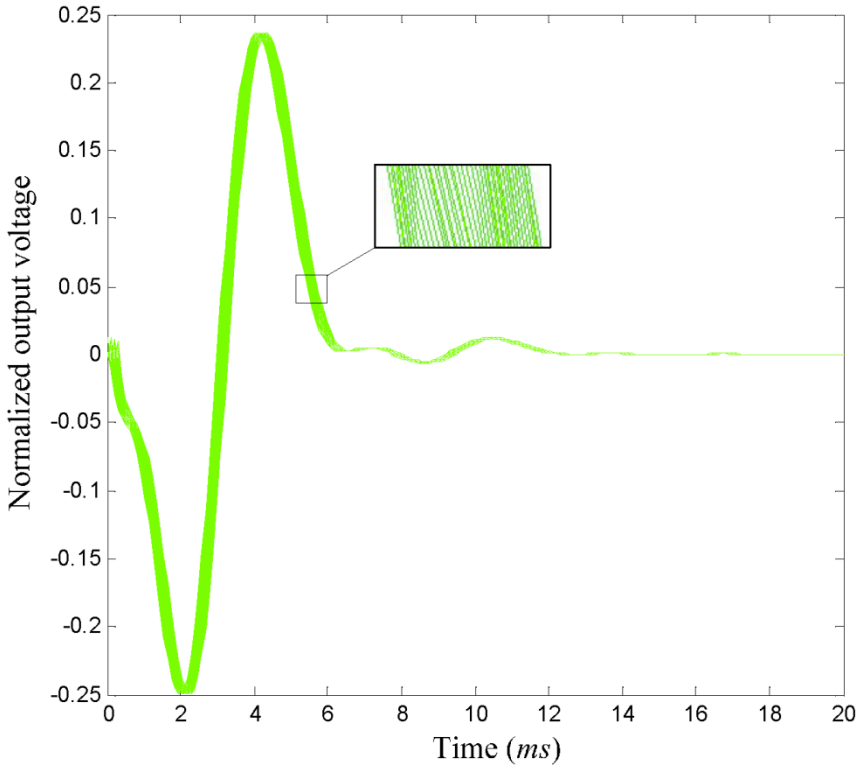

FIGURE 11 Temperature sweep analysis of the designed wavelet circuit (σ=1)

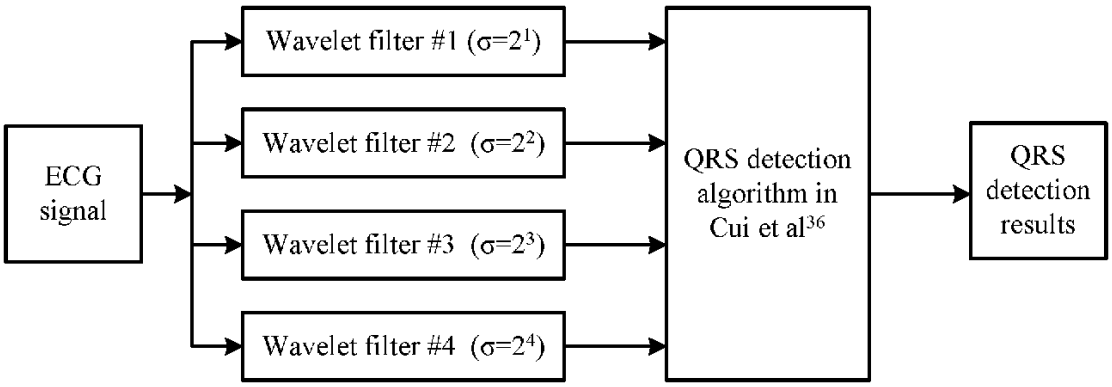

FIGURE 12 Block diagram of QRS detection based on wavelet filters

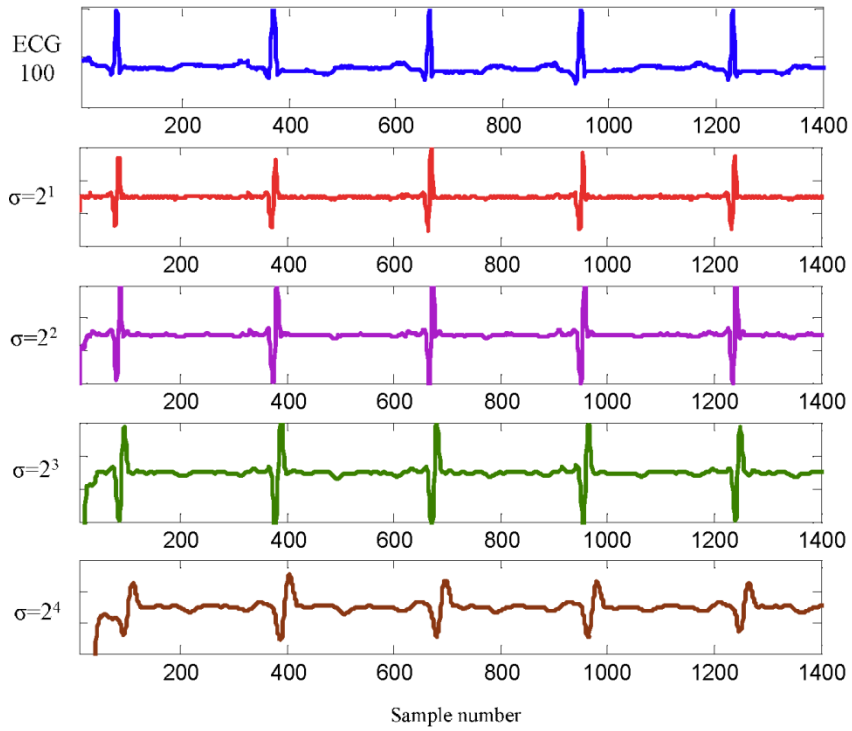

FIGURE 13 ECG 100 signal and the outputs of wavelet filters with four scales

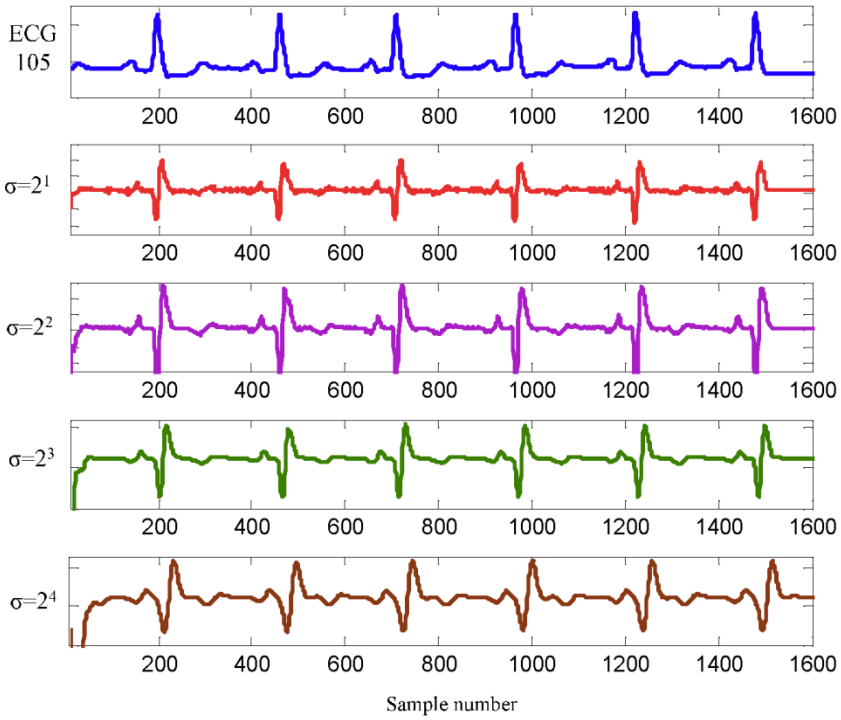

FIGURE 14 ECG 105 signal with baseline drift and much noise, and the outputs of wavelet filters with four scales